https://doi.org/10.5194/hess-2020-380
Preprint. Discussion started: 17 August 2020

Hydrology and Earth System Sciences
Discussions

Sigmoidal Water Retention Function with Improved Behavior in Dry and Wet Soils

Gerrit H. de Rooij, Juliane Mai, and Raneem Madi

G.H. de Rooij and R. Madi, Helmholtz Centre for Environmental Research – UFZ GmbH, Soil System Science Dept., Theodor–Lieser–Strasse 4, 06120 Halle (Saale), Germany; R. Madi, current address: GFI Grundwasser–Consulting–Institut GmbH, Meraner Strasse 10, 01217 Dresden, Germany.

J. Mai, University of Waterloo, Dept. Civil and Environmental Engineering, 200 University Ave West, Waterloo, ON N2L 3G1, Canada.

Corresponding author: G.H. de Rooij (gerrit.derooij@ufz.de)

https://doi.org/10.5194/hess-2020-380
Preprint. Discussion started: 17 August 2020

Hydrology and Earth System Sciences
Discussions

Abstract

A popular parameterized soil water retention curve (SWRC) has a hydraulic conductivity curve associated with it that can have an infinite slope at saturation. The problem was eliminated before by giving the SWRC a non–zero air–entry value. This improved version still has an asymptote at the dry end, which limits its usefulness for dry conditions and causes its integral to diverge for commonly occurring parameter values. We therefore joined the parameterizations' sigmoid mid–section to a logarithmic dry section ending at zero water content for a finite matric potential, as was done previously for a power–law type SWRC. We selected five SWRC parameterizations that had been proven to produce unproblematic near–saturation conductivities and fitted these and our new curve to data from 21 soils. The logarithmic dry branch gave more realistic extrapolations into the dry end of both the retention and the conductivity curves than an asymptotic dry branch. We tested the original curve, its first improvement, and our second improvement by feeding them into a numerical model that calculated evapotranspiration and deep drainage for nine combinations of soils and climates. The new curve was more robust than the other two. The new curve was better able to produce a conductivity curve with a substantial drop during the early stages of drying than the earlier improvement. It therefore generated smaller amounts of more evenly distributed deep drainage compared to the spiked response to rainfall produced by the earlier improvement.

https://doi.org/10.5194/hess-2020-380
Preprint. Discussion started: 17 August 2020

Hydrology and Earth System Sciences
Discussions

Introduction

The soil water retention function introduced by van Genuchten (1980) has been the most popular parameterization (denoted VGN below; these and other abbreviations are listed in Appendix A) to describe the SWRC in numerical models for unsaturated flow for the past few decades (e.g., Kroes et al., 2017; Šimůnek and Bradford, 2008; Šimůnek et al., 2016):

$$\theta(h) = \theta_r + (\theta_s - \theta_r)(1 + |\alpha h|^n)^{\frac{1}{n}-1}, \quad h \leq 0 \tag{1}$$

where h denotes the matric potential in equivalent water column [L]. The volumetric water content is denoted by θ, with the subscript 's' denoting its value at saturation and the subscript 'r' its residual, or irreducible, value. Parameters α [L^{-1}] and n are shape parameters.

Van Genuchten (1980) combined Eq. (1) with Mualem's (1976) conductivity model and derived an analytical expression for the unsaturated hydraulic conductivity curve:

$$K(h) = K_s \frac{\left[1-|\alpha h|^{n-1}(1+|\alpha h|^n)^{\frac{1}{n}-1}\right]^2}{(1+|\alpha h|^n)^{\frac{1}{2}-\frac{1}{2n}}} \tag{2}$$

where K[LT^{-1}] is the soil hydraulic conductivity and K_s [LT^{-1}] its value at saturation.

Hysteretic (Kool and Parker, 1987) and multimodal versions (Durner, 1994) of Eq. (1) are available. Apart from the convenience of having analytical expressions for the retention as well as the conductivity curve, the function's popularity derives from its

https://doi.org/10.5194/hess-2020-380
Preprint. Discussion started: 17 August 2020


Hydrology and Earth System Sciences
Discussions

continuous derivative and its inflection point, which gives it considerable flexibility in fitting observations.

Fuentes et al. (1991) warned that the asymptotic residual water content at the dry end could lead to a non–converging integral of the retention curve, and showed how this would mathematically lead to a physically impossible unlimited water uptake capacity of a finite soil column. From their analysis follows that this can only be prevented if $n > 2$ in Eq. (1), a condition which is often not satisfied.

Near saturation, the slope $\mathrm{d}\theta/\mathrm{d}h$ is not zero at zero matric potential. This implies that the soil has pores that have at least one infinite principal radius according to the Laplace–Young Law (Hillel, 1998, p. 46), which is physically unacceptable (see also Iden et al., 2015). Durner (1994) noted this could lead to an infinite slope in the hydraulic conductivity function of Mualem (1976) when the matric potential approached zero, and Ippisch et al. (2006) showed that if $n < 2$ this would indeed be the case. The more recent sigmoid curve of Fredlund and Xing (1994) and its modification by Wang et al. (2016), used by Wang et al. (2018) and Rudiyanto et al. (2020) have the same problem (see Appendix B for the proof). The curve of Assouline et al. (1998) is based on the Weibull distribution, and therefore has a non–zero slope at zero matric potential when its fitting parameter η is smaller than 2, which was the case for 75% of the soils for which it was fitted. None of these curves therefore offers a remedy to the problem associated with VGN.

Corrections for the conductivity curve were proposed by Vogel et al. (2001), Schaap and van Genuchten (2006), and Iden et al. (2015), but these leave the effect of the non–physical, very large pores on the SWRC intact and create an inconsistency between the retention model and the conductivity model. For instance, Iden et al. (2015) clipped the

https://doi.org/10.5194/hess-2020-380
Preprint. Discussion started: 17 August 2020


Hydrology and Earth System Sciences
Discussions

integral in the conductivity function at a matric potential h_c somewhat below zero. In the range between h_c and zero, their modified unsaturated hydraulic conductivity increased linearly with the water content (Iden et al. (2015), Fig. 1), which is not physically realistic because the pore sizes that are being filled are increasing in size according to Eq. (1) or its multimodal version (Peters et al., 2011). Only Ippisch et al. (2006) addressed the underlying problem in the SWRC by introducing a non–zero air–entry value, thereby eliminating excessively large pores whilst maintaining the mathematical consistency between the expressions for the retention and the conductivity curves. In doing so they sacrificed the continuity of the derivative of the VGN curve. Iden et al. (2015) suspected this would pose a challenge to numerical solves of Richards' equation, but Ippisch et al.'s (2006) numerical simulations ran without difficulty. Their equation scaled the sigmoid curve by its value at the air–entry value h_{ae} [L] and introduced a saturated section for $h > h_{ae}$.

$$\theta(h) = \begin{cases} \theta_r + (\theta_s - \theta_r)\left(\frac{1+|\alpha h|^n}{1+|\alpha h_{ae}|^n}\right)^{\frac{1}{n}-1}, & h \le h_{ae} \\ \theta_s, & h > h_{ae} \end{cases} \quad (3)$$

This function is denoted VGA below.

The smooth, sigmoidal shape of VGN resembles many observed curves for which the data points in the wet range were obtained by equilibrating cylindrical soil samples at well–defined matric potentials and determining the corresponding water content by weighing the sample (Klute, 1986, p. 644–647). Liu and Dane (1995) took into account the vertical variation of the water content in such samples and demonstrated that a power–law SWRC with a well–defined air–entry matric value but without inflection point can produce a

https://doi.org/10.5194/hess-2020-380
Preprint. Discussion started: 17 August 2020


Hydrology and Earth System Sciences
Discussions

sigmoid–type apparent SWRC if the non–uniform distribution of water in the sample is ignored. A series of data points suggesting a smooth SWRC therefore does not intrinsically contradict the existence of a discrete non–zero air–entry value, corroborating the correction to VGN by Ippisch et al. (2006).

In a separate development, several researchers argued that in the dry range, water is bound to the soil by adsorptive rather than capillary forces. Usually, a logarithmic term that allowed the adsorbed water content to go to zero at a prescribed matric potential was added to a capillary term. The former would dominate in the dry range and become negligible as the soil became wetter (e.g., Campbell and Shiozawa, 1992; Fayer and Simmons, 1995; Khlosi et al., 2006; Peters, 2013). The logarithmic relationship was based on the sorption theory of Bradley (1936). It removed the asymptote and the associated problem of the non–converging integral of the SWRC that Fuentes et al. (1991) warned about. Rossi and Nimmo (1994) presented a junction model in which a critical matric potential separated purely capillary bound water (described by a variation of the Brooks–Corey (1964) model) from solely adsorbed water. By doing so they avoided the problem of many of the other models that would have some capillary bound water still present in the soil below the matric potential at which the adsorbed water content had gone to zero.

Madi et al. (2018) generalized the analysis of Ippisch et al. (2006) and applied it to 18 parameterizations of the SWRC to verify that the slope of the hydraulic conductivity near saturation would remain finite. Apart from Eq. (3), only the expressions developed by Brooks and Corey (1964) (denoted BCO), Fayer and Simmons (1995) (denoted FSB), and the junction model of Rossi and Nimmo (1994) (denoted RNA) satisfied this requirement. In the latter case, the equation had to be modified by removing a modification that

https://doi.org/10.5194/hess-2020-380
Preprint. Discussion started: 17 August 2020


Hydrology and Earth System Sciences
Discussions

124 smoothed the curve near saturation. All these equations have a power law relationship
125 between the water content and the matric potential, and therefore do not have the sigmoid
126 shape of VGN and VGA.

127 As noted above, the introduction of a non–zero air–entry value by Ippisch et al.
128 (2006) eliminated the unphysically large slopes of the hydraulic conductivity according to
129 Mualem (1976). The approach of Rossi and Nimmo (1994) resolved the issue of the
130 asymptotic behavior in the dry range. The objective of this paper therefore is to combine
131 Rossi and Nimmo's (1994) model for the dry range with the VGA model of Ippisch et al.
132 (2006) to arrive at a SWRC (denoted RIA) that has a non–zero air–entry value, a sigmoid
133 shape in the intermediate range, a dry branch that can reach zero water content at a finite
134 matric potential, and therefore a finite integral. We will also develop an explicit expression
135 for the unsaturated hydraulic conductivity based on this SWRC. For completeness, a
136 generalized expression for multimodal SWRCs will also be derived.

137 Together with the other functions that lead to physically acceptable behavior of the
138 hydraulic conductivity near saturation (BCO, FSB, RNA, and VGA), RIA will be fitted to 21
139 soils selected from the UNSODA database (National Agricultural Library, 2017; Nemes et al.,
140 2001) that cover a wide range of textures (Madi et al., 2018). For comparison VGN is also
141 included, in view of its de facto status as the standard parameterization for the SWRC. All
142 three versions with the sigmoid shape (VGN, VGA, and RIA) will be tested in a simulation
143 study for different combinations of soil types and climates.

144

145 Theory

146 The Soil Water Retention Curve

https://doi.org/10.5194/hess-2020-380
Preprint. Discussion started: 17 August 2020


Hydrology and Earth System Sciences
Discussions

147 The junction model of Rossi and Nimmo (1994) has a SWRC with a logarithmic dry
148 branch without residual water content. The parameterization proposed by Ippisch et al.
149 (2006) combines the sigmoid shape of van Genuchten (1980) with a non–zero air–entry
150 value. By setting the θ_r in Ippisch et al. (2006) to zero, we can combine the two models to
151 give the following parameterization:
152

153 $$\theta(h) = \begin{cases} 0, & h \le h_\mathrm{d} \\ \theta_\mathrm{s}\beta \ln\left(\frac{h_\mathrm{d}}{h}\right), & h_\mathrm{d} < h \le h_\mathrm{j} \\ \theta_\mathrm{s}\left(\frac{1+|\alpha h|^n}{1+|\alpha h_\mathrm{ae}|^n}\right)^{\frac{1}{n}-1}, & h_\mathrm{j} < h \le h_\mathrm{ae} \\ \theta_\mathrm{s}, & h > h_\mathrm{ae} \end{cases} \quad (4)$$

154
155 where subscripts ‘d’ and ‘ae’ denote the value at which the water content reaches zero and
156 the air–entry value, respectively, and subscript ‘j’ indicates the value at which the
157 logarithmic and sigmoid branch are joined. Joining instead of adding the the logarithmic
158 and the sigmoid functions avoids potentially non-monotonic behavior (Peters et al., 2011).
159 The derivative of Eq. (4) is
160

161 $$\frac{\mathrm{d}\theta}{\mathrm{d}h}(h) = \begin{cases} 0, & h \le h_\mathrm{d} \\ \frac{\theta_\mathrm{s}\beta}{h}, & h_\mathrm{d} < h \le h_\mathrm{j} \\ \theta_\mathrm{s}\alpha(n-1)|\alpha h|^{n-1}(1+|\alpha h_\mathrm{ae}|^n)^{1-\frac{1}{n}}(1+|\alpha h|^n)^{\frac{1}{n}-2}, & h_\mathrm{j} < h \le h_\mathrm{ae} \\ 0, & h > h_\mathrm{ae} \end{cases} \quad (5)$$

162
163 Mass continuity dictates that the SWRC is continuous. At the air–entry value, this condition
164 is met irrespective of the parameter values. At h_j, continuity requires the following equality
165 to hold:

https://doi.org/10.5194/hess-2020-380
Preprint. Discussion started: 17 August 2020


Hydrology and Earth System Sciences
Discussions

$$\beta \ln\left(\frac{h_d}{h_j}\right) = \left(\frac{1+|\alpha h_j|^n}{1+|\alpha h_{ae}|^n}\right)^{\frac{1}{n}-1} \quad (6)$$

In accordance with Rossi and Nimmo (1994) we also require the derivatives at h_j to match, leading to

$$\beta = (n-1)\left|\alpha h_j\right|^n (1+|\alpha h_{ae}|^n)^{1-\frac{1}{n}} \left(1+\left|\alpha h_j\right|^n\right)^{\frac{1}{n}-2} \quad (7)$$

Combining Eqs. (6) and (7) and solving for h_d gives:

$$h_d = h_j \exp\left(\frac{1+|\alpha h_j|^{-n}}{n-1}\right) \quad (8)$$

This leaves h_{ae}, h_j, θ_s, α, and n as fitting parameters.

The derivation of a multimodal curve analogous to that of Durner (1994) and Zurmühl and Durner (1998) is straightforward if the values of h_{ae} and h_j are kept the same for all contributing terms:

$$\theta(h) = \begin{cases} 0, & h \le h_d \\ \theta_s \beta \ln\left(\frac{h_d}{h}\right), & h_d < h \le h_j \\ \theta_s \sum_{i=1}^{k} w_i \left(\frac{1+|\alpha_i h|^{n_i}}{1+|\alpha_i h_{ae}|^{n_i}}\right)^{\frac{1}{n_i}-1}, & h_j < h \le h_{ae} \\ \theta_s, & h > h_{ae} \end{cases} \quad (9)$$

https://doi.org/10.5194/hess-2020-380
Preprint. Discussion started: 17 August 2020


Hydrology and Earth System Sciences
Discussions

where the modality is indicated by k. The weighting factors w_i are bounded on the interval [0,1] and their sum must equal 1 (Durner, 1994; Zurmühl and Durner, 1998). Requiring the logarithmic and the multimodal branch as well as their derivatives to match at h_j leads to

$$\beta = \sum_{i=1}^{k} w_i (n_i - 1)\left|\alpha_i h_j\right|^{n_i} \left(1 + \left|\alpha_i h_{ae}\right|^{n_i}\right)^{1-\frac{1}{n_i}} \left(1 + \left|\alpha_i h_j\right|^{n_i}\right)^{\frac{1}{n_i}-2} \quad (10)$$

and

$$h_d = h_j \exp\left[\frac{\sum_{i=1}^{k} w_i \left(1+\left|\alpha_i h_{ae}\right|^{n_i}\right)^{1-\frac{1}{n_i}} \left(1+\left|\alpha_i h_j\right|^{n_i}\right)^{\frac{1}{n_i}-1}}{\sum_{i=1}^{k} w_i (n_i-1)\left|\alpha_i h_j\right|^{n_i} \left(1+\left|\alpha_i h_{ae}\right|^{n_i}\right)^{1-\frac{1}{n_i}} \left(1+\left|\alpha_i h_j\right|^{n_i}\right)^{\frac{1}{n_i}-2}}\right] \quad (11)$$

The fitting parameters are h_{ae}, h_j, θ_s, α_i, n_i, and w_i.

The Unsaturated Hydraulic Conductivity Curve

Kosugi (1999) proposed the following conductivity model (see also Ippisch et al., 2006):

$$K(h) = K\left(h(S_e)\right) = \begin{cases} K_s S_e^{\tau} \left(\frac{\int_{-\infty}^{h(S_e)} |h|^{-\kappa} \frac{dS}{dh} dh}{\int_{-\infty}^{h_{ae}} |h|^{-\kappa} \frac{dS}{dh} dh}\right)^{\gamma}, & h < h_{ae} \\ K_s, & h \geq h_{ae} \end{cases} \quad (12)$$

with γ, κ, and τ denoting shape parameters, S_e denoting the degree of saturation, and S representing a variable running over all values of the degree of saturation from zero to its

https://doi.org/10.5194/hess-2020-380
Preprint. Discussion started: 17 August 2020


Hydrology and Earth System Sciences
Discussions

actual value S_e. Mualem's (1976) conductivity model is a special case of Eq. (11), with $\gamma = 2$, $\kappa = 1$, and $\tau = 0.5$.

The integrals in Eq. (12) that arise when Eq. (5) is used to find $\mathrm{d}S/\mathrm{d}h$ can be evaluated analytically if $\kappa = 1$. The resulting conductivity function is

$$K(h) = \begin{cases} 0, & h \le h_\mathrm{d} \\ K_\mathrm{s}\left(\beta \ln\left|\frac{h_\mathrm{d}}{h}\right|\right)^{\tau}\left[\frac{\frac{\beta}{|h_\mathrm{d}|}-\frac{\beta}{|h|}}{\frac{\beta}{|h_\mathrm{d}|}-\frac{\beta}{|h_\mathrm{j}|}+\frac{|\alpha h_\mathrm{ae}|^n}{|h_\mathrm{ae}|}-(1+|\alpha h_\mathrm{ae}|^n)^{1-\frac{1}{n}}F(h_\mathrm{j})}\right]^{\gamma}, & h_\mathrm{d} < h \le h_\mathrm{j} \\ K_\mathrm{s}\left(\frac{1+|\alpha h|^n}{1+|\alpha h_\mathrm{ae}|^n}\right)^{\frac{\tau}{n}-\tau}\left\{\frac{\frac{\beta}{|h_\mathrm{d}|}-\frac{\beta}{|h_\mathrm{j}|}+(1+|\alpha h_\mathrm{ae}|^n)^{1-\frac{1}{n}}\left[F(h)-F(h_\mathrm{j})\right]}{\frac{\beta}{|h_\mathrm{d}|}-\frac{\beta}{|h_\mathrm{j}|}+\frac{|\alpha h_\mathrm{ae}|^n}{|h_\mathrm{ae}|}-(1+|\alpha h_\mathrm{ae}|^n)^{1-\frac{1}{n}}F(h_\mathrm{j})}\right\}^{\gamma}, & h_\mathrm{j} < h \le h_\mathrm{ae} \\ K_\mathrm{s}, & h > h_\mathrm{ae} \end{cases} \quad (13a)$$

where

$$F(h) = \frac{|\alpha h|^n (1+|\alpha h|^n)^{\frac{1}{n}-1}}{|h|} \quad (13b)$$

Other conductivity models are available and can be selected if desired, for instance using the framework presented by Weber et al. (2019).

https://doi.org/10.5194/hess-2020-380
Preprint. Discussion started: 17 August 2020


Hydrology and Earth System Sciences
Discussions

219 The conductivity function associated with the multimodal soil water retention
220 function cannot be expressed in analytical form. For that case, the degree of saturation for
221 any h can be found with Eq. (9) and the corresponding hydraulic conductivity determined
222 with Eq. (12) or another conductivity model.
223

224 Materials and Methods

225 We selected 21 soils from the UNSODA database that had sufficient retention data
226 and together covered the textures represented in UNSODA. We then fitted Eq. (4) to these
227 soils using a Shuffled Complex Evolution algorithm (see Madi et al. (2018) and Appendix C
228 for details of the algorithm and the fitting procedure). We slightly modified the fitting code
229 used by Madi et al. (2018) to generate output that can more readily be converted to the
230 MATER.IN input file for Hydrus–1D, the numerical model used in this study. We therefore
231 refitted BCO, FSB, RNA, VGN, and VGA as well.
232 One–dimensional simulations for all combinations of three soils and three climates
233 were carried out to examine how the choice of parameterization affected fluxes at the soil
234 surface and in the subsoil. The model Hydrus–1D version 4.16.0110 (Šimůnek et al., 2013,
235 PC-progress website) was used for this purpose. The selected soils were a loamy sand
236 (UNSODA identifier: 2104), a silty loam (3261), and a clay (1181). Weather records were
237 generated from climate parameters based on weather data from Colombo (Sri Lanka,
238 monsoon climate), Tamale (Ghana, semi–arid climate), and Ukkel (Belgium, temperate
239 climate). Table 1 gives the most relevant statistics of the weather records. In order to
240 highlight the effects of the air–entry value and the logarithmic dry end of the SWRC, we
241 used the sigmoidal VGN, VGA, and RIA parameterizations in the simulations. The

https://doi.org/10.5194/hess-2020-380
Preprint. Discussion started: 17 August 2020

Hydrology and Earth System Sciences
Discussions
Open Access
EGU

242 Supplement details the generation of the weather records, the set–up of the simulations,
243 and the simulation results.

244

245 Table 1. Average cumulative monthly and annual rainfall and potential evapotranspiration
246 of the three test climates calculated from 1000–year generated weather records.

	Monsoon		Semi–arid		Temperate	
Month	Rain (mm)	ET_{pot} (mm)	Rain (mm)	ET_{pot} (mm)	Rain (mm)	ET_{pot} (mm)
Jan	94.0	160.5	14.3	159.4	69.0	12.7
Feb	83.3	156.0	12.9	158.1	55.6	18.8
Mar	217.6	166.8	13.7	185.0	59.4	34.4
Apr	233.8	160.0	34.1	177.7	57.1	51.1
May	237.4	164.0	117.6	166.6	24.5	73.9
Jun	138.5	164.7	140.9	151.4	24.4	83.3
Jul	139.4	172.4	141.8	153.2	23.2	86.3
Aug	137.1	174.4	213.5	145.0	20.9	73.7
Sep	133.0	164.7	214.7	136.9	23.8	50.6
Oct	325.8	142.3	76.6	154.1	38.0	30.8
Nov	328.8	128.1	12.9	149.3	49.1	16.1
Dec	112.0	150.9	12.9	151.9	51.2	11.2
Annual sum	2180.5	1904.8	1005.8	1888.7	496.1	542.9

247

248

https://doi.org/10.5194/hess-2020-380
Preprint. Discussion started: 17 August 2020

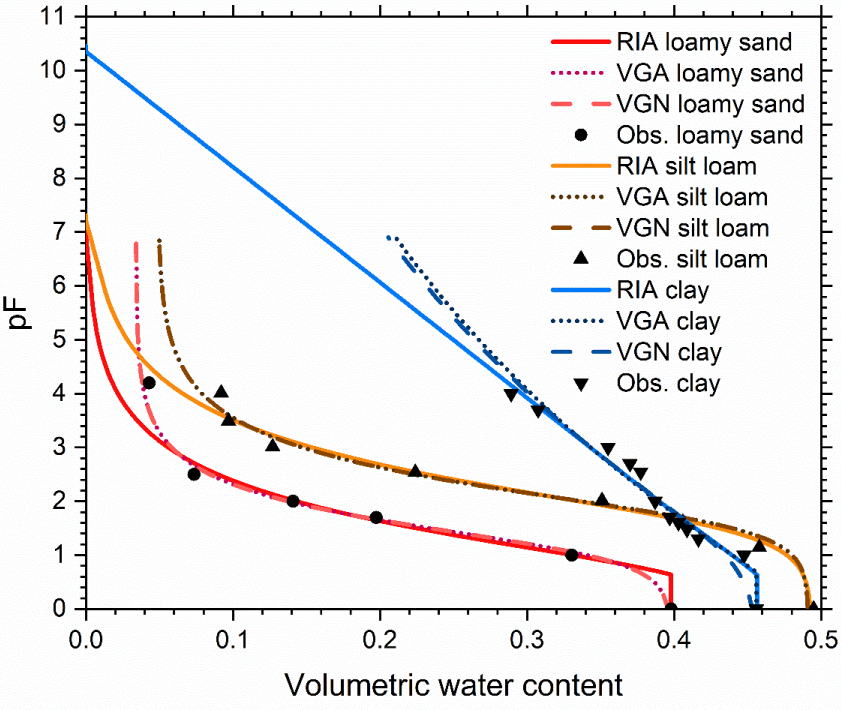

Figure 1. Soil water retention data of the soils used in the numerical simulations, and the retention curves fitted to these data for three parameterizations with a sigmoid midsection of the curve: the original model by van Genuchten (1980) (VGN), the modification thereof by Ippisch et al. (2006) (VGA), and the further modification introduced in this paper (RIA).

The different parameterizations of the SWRCs (Table 2, Fig. 1) were used to generate tables of the soil water retention and conductivity curves that were provided as input to Hydrus–1D. Mualem's (1976) model for the unsaturated soil hydraulic conductivity was used to generate relative hydraulic conductivities (scaled by K_s). These were converted to

https://doi.org/10.5194/hess-2020-380
Preprint. Discussion started: 17 August 2020

unscaled conductivities (Fig. 2) by multiplying with the K_s–value according to the UNSODA database, and then included in the tables.

Table 2. Parameters of the fit to data of the three parameterizations of the soil water retention curve used for the numerical simulations.

Soil	Parameter	θ_r	θ_s	α (cm^{-1})	n	h_{ae} (cm)	h_j (cm)
Clay	RIA	–	0.45666	0.70200	1.0543	–4.2523	–205.65
	VGA	2.12×10^{-6}	0.45603	1.7047	1.0543	–4.8324	–
	VGN	3.34×10^{-6}	0.45616	0.14265	1.0571	–	–
Silt loam	RIA	–	0.49346	0.023340	1.3691	-2.361×10^{-3}	-1.0739×10^{6}
	VGA	0.048871	0.49122	0.018365	1.5158	-2.081×10^{-3}	–
	VGN	0.048816	0.49134	0.018425	1.5149	–	–
Loamy sand	RIA	–	0.39801	0.17096	1.4106	–4.3581	-7.7464×10^{5}
	VGA	0.034209	0.39771	0.069661	1.6395	–0.016234	–
	VGN	0.034133	0.39772	0.069707	1.6389	–	–

For the clay soil, the recorded value (178 cm d^{-1}) was such that it can be assumed that macropore flow contributed to its value. We therefore also ran simulations with a K_s – value of 1.25 cm d^{-1}. This value was adopted from soil 1182 from the UNSODA database, from the same location.

https://doi.org/10.5194/hess-2020-380
Preprint. Discussion started: 17 August 2020

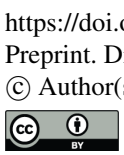

Hydrology and Earth System Sciences
Discussions

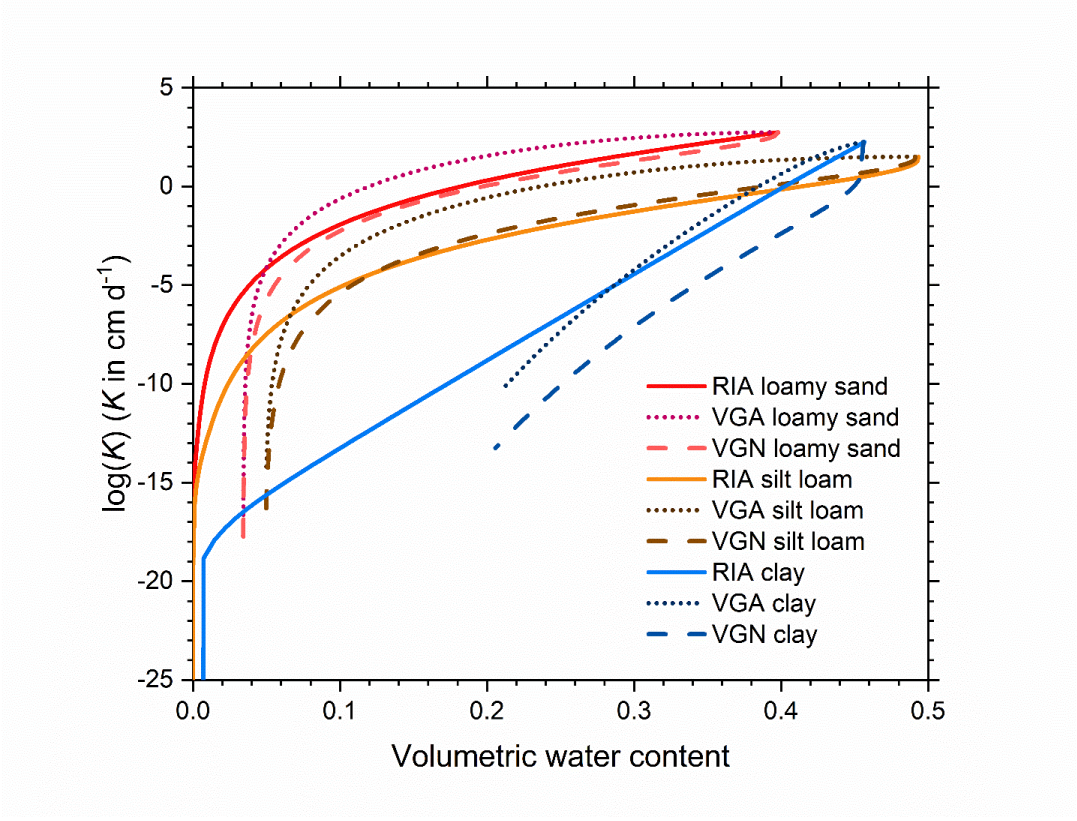

Figure 2. The unsaturated soil hydraulic conductivity curves derived from the fitted retention curves depicted in Fig.1 and scaled by soil–specific values of the hydraulic conductivity at saturation.

Results and Discussion

Fitted Curves for 21 Soils

The fitted parameter values (Tables C1–C4) and the associated curves (Figs. C2–C5) are presented in Appendix C. The extra parameter of RIA compared to RNA and FSB gives it a clear advantage in fitting the full water content range. The sigmoid shape of RIA provides a better fit near the air entry value while still providing good fits of the drier data points

https://doi.org/10.5194/hess-2020-380
Preprint. Discussion started: 17 August 2020


Hydrology and Earth System Sciences
Discussions

(e.g. 1121 in Fig. C3, all soils in Figs. C4–C5). In the wet range, the sigmoid curves (VGN, VGA, RIA) outperform the power–law curves (BCO, FSB, RNA). In almost all cases, VGA and RIA look very similar. Figure C3 shows multimodality in the data for five out of six soils that cannot be reproduced by any of the parameterizations.

Many of the UNSODA soils have one retention data point at saturation and the next at $h = -10$ cm. The air–entry value of many sandy soils is within that range. The fitting routine struggles to fit h_{ae} to these data for VGA and RIA because the sigmoid shape of the van Genuchten parameterization has such flexibility that it can fit the intermediate range well for a range of h_{ae}–values. We therefore recommend making $\theta(h)$–measurements at one or two matric potentials between zero and −10 cm for coarse–textured soils.

Eleven of the 21 soils have residual water contents for VGN and/or VGA that exceed 0.05 (up to 0.263), mostly in loamy sands, loams, and clays (Tables C1–C4). All of these and several others have dry–end data points with water contents that appear too high (Figs. C2–C5). These water contents may have been overestimated due to the lack of equilibrium reported by Bitelli and Flury (2009). The parameterizations without asymptote (FSB, RNA, RIA) generally have more plausible fits based on visual inspection of the graphs, but because they do not follow the upward tail of the data in the dry end, their RMSE values for the cases with suspicious dry–end data points are larger than those of VGN and VGA (Tables C5–C8).

Especially for fine–textured soils, the lack of data points for air dryness or oven dryness (Figs. C3–C5) causes the fitting procedure to treat θ_r for the asymptotic dry branches and h_d for the logarithmic dry branches as pure fitting parameters for the drier range of the data. This range exceeds pF4.2 in only one case and in several cases likely

https://doi.org/10.5194/hess-2020-380
Preprint. Discussion started: 17 August 2020


Hydrology and Earth System Sciences
Discussions

suffers from lack of equilibrium (Bitelli and Flury, 2009). This leads to unrealistically high values for both in many cases. If applications are envisioned for which low water contents are expected, it would be better to have some data in the dry range and ensure equilibrium has been achieved before fitting RIA. One could even add a virtual data point with zero water content at pF6.8, since this is the value that is approximated by many laboratory ovens (Schneider and Goss, 2012). We did not do so here to be able to observe how the various parameterizations perform on frequently reported data ranges.

Figure C5 showcases a peculiarity of FSB. The original version by Fayer and Simmons (1995) allowed capillary bound water to be present even if the adsorbed water content was down to zero. We adopted the correction by Madi et al. (2018, Eq. (S12a)) that forced the amount of water bound by capillary forces to zero if the adsorbed water content goes reaches zero at pF6.8. In the case of clay soils, the parameter values are such that a substantial amount of capillary bound water is still present at pF6.8, leading to a sudden cut–off at pF6.8.

The hydraulic conductivity curves based on water retention curve parameters and K_s very poorly match the data in most cases (Fig. C6–C9). We note here that all but one (soil 4450, Fig. C8) sets of unsaturated conductivity data were obtained in the field, while all retention data were laboratory data on drying samples. The reported K_s–values were probably measured in a separate experiment (possibly in the laboratory), in which case a mismatch between K_s and the unsaturated conductivity data is to be expected. The poor match with field data notwithstanding, the graphs can be used to study the effect of the parameterization on the shape of the $K(\theta)$ curve. The comparison between measured and modeled shapes of the conductivity curves is inconclusive.

https://doi.org/10.5194/hess-2020-380
Preprint. Discussion started: 17 August 2020


Hydrology and Earth System Sciences
Discussions

In many soils, regardless of texture, RIA's $K(\theta)$ curve drops of much slower in the dry range than those of VGN and VGA (Fig. C6–C9), a consequence of the ability of the underlying SWRC to reach zero water content at a finite matric potential. Near saturation, RIA's $K(\theta)$ curve often drops off sharply before leveling off, in stark contrast to that of VGA, which remains high in the wet range. Given the similarity in the $\theta(h)$ curves of VGA and RIA, the difference in their $K(\theta)$ curves is remarkable. RIA's $K(\theta)$ curve is the only one that can drop off sharply near saturation, level out somewhat in the mid-range and drop ever more sharply in the dry range. It is below many of the other curves in the wet and mid-range, and above most of them in the dry range.

Peters et al. (2011) developed parameter constraints to ensure physically plausible shapes of the SRWC and the conductivity curve. For FSB, the criterion for non-monotonicity of the conductivity curve is not met for soil 4450 (Fig. C8), resulting in K increasing with decreasing water content near saturation.

Model Simulations

In total, 21 out of 36 combinations of soil–climate–parameterization ran to completion. Runoff did not occur in any of the successful model runs. Convergence was not achieved for any of the runs for the clay soil with the reduced K_s–value. For the clay soil with the high K_s–value, only RIA ran to completion. The discontinuity of the first derivative at the air-entry value did not cause numerical problems. In fact, the replacement of any parametric expression by a look-up table creates a discontinuity of the first derivative at every point of the look-up table.

https://doi.org/10.5194/hess-2020-380
Preprint. Discussion started: 17 August 2020


Hydrology and Earth System Sciences
Discussions

Table 3 lists the main mean annual fluxes calculated from the simulation study. The median flux was produced by RIA for all combinations of soil and climate. The mean annual actual transpiration between the three parameterizations differed by more than 10% from the median only for the loamy sand under a temperate climate. Actual evaporation never deviated more than 10%. The amount of water leaving the soil profile differed substantially between parameterizations for the semi-arid and temperature, especially for VGA (20–46% deviation from the median).

The daily data revealed significant differences on smaller time scales that will be relevant if reactive solute transport is of interest (see the Supplement). The fluxes generated by the VGA parameterizations responded more quickly and strongly to the rainfall signal, with VGN and RIA giving a more delayed and smooth response. The SWRCs (Fig. 1) offer no explanation for this, but Fig. 2 shows that VGA's hydraulic conductivity in the wet and intermediate water content range for all three soils is considerably higher than that of VGN and RIA, except for clay, where it is only moderately higher than RIA's and drops below RIA at a water content of 0.28. Thus, small differences between SWRCs can have a significant influence on soil water flow simulations through their effect on the soil hydraulic conductivity curve, an effect that the reviews by Leij et al. (1997) and Assouline and Or (2013) took into consideration to some degree, but was not considered in several other studies that compared different parameterizations (e.g., Rossi and Nimmo, 1994; Assouline et al., 1998; Cornelis et al., 2005; Khlosi et al., 2008).

https://doi.org/10.5194/hess-2020-380
Preprint. Discussion started: 17 August 2020

Hydrology and Earth System Sciences
Discussions

369 Table 3. Average of the annual sums of the actual transpiration and evaporation, and of the
370 outflow across the lower boundary of the simulated soil profiles. The averages were
371 calculated for the final six years of the simulation periods. The values in parentheses are
372 scaled with respect to the corresponding value for RIA.

Climate	Soil	Actual transpiration (mm)			Actual evaporation (mm)			Downward flux at 2 m depth (mm)		
		RIA	VGA	VGN	RIA	VGA	VGN	RIA	VGA	VGN
Monsoon	clay	962	–	–	543	–	–	876	–	–
	silt loam	1114	1044 (0.94)	1112 (1.06)	541	554 (1.02)	534 (0.96)	711	763 (1.07)	718 (0.94)
	loamy sand	1037	976 (0.94)	1024 (1.05)	480	440 (0.92)	461 (1.05)	863	959 (1.11)	896 (0.93)
Semi–arid	clay	585	–	–	319	–	–	294	–	–
	silt loam	657	588 (0.90)	653 (1.11)	297	303 (1.02)	287 (0.95)	164	226 (1.37)	177 (0.78)
	loamy sand	585	540 (0.92)	572 (1.06)	248	222 (0.89)	234 (1.06)	290	363 (1.25)	319 (0.88)
Temperate	clay	202	–	–	163	–	–	167	–	–
	silt loam	281	236 (0.84)	271 (1.15)	150	151 (1.01)	143 (0.95)	99	144 (1.46)	114 (0.79)
	loamy sand	224	205 (0.92)	214 (1.04)	130	118 (0.91)	124 (1.05)	174	208 (1.20)	190 (0.91)

373

https://doi.org/10.5194/hess-2020-380
Preprint. Discussion started: 17 August 2020


Hydrology and Earth System Sciences
Discussions

Summary and Conclusions

The improvements incorporated in the RIA parameterization for the first time remove problems of the popular VGN model in both the wet and the dry range while retaining the desirable sigmoid shape in the mid–range. This shape allows its multimodal version to represent SWRCs with multiple humps. RIA offers a wider range of shapes for the conductivity curve than any other parameterization that does not lead to the unphysical behavior near saturation that was revealed by Durner (1994) and Ippisch et al. (2006) for VGN and by Madi et al. (2018) for 14 other parameterizations. RIA also proved to be more robust during numerical simulations than VGN itself as well as its modification VGA, which still has a non–physical asymptote at a non–zero residual water content. The deep drainage generated by RIA was more spread out and smaller than the spiked response to rainfall produced by VGA, probably because RIA was better able to produce a conductivity curve with a substantial drop during the early stages of drying. We therefore hope that RIA or its multimodal version will be adopted for use in numerical simulations of soil water flow. The catalogue of parameters for 21 soils in Appendix C may be of help for such simulations.

https://doi.org/10.5194/hess-2020-380
Preprint. Discussion started: 17 August 2020


Hydrology and Earth System Sciences
Discussions

Appendix A. List of Abbreviations

BC: Brooks and Corey (1964)

BCO: parameterization of the SWRC according to the original Brooks and Corey (1964) equation

FSB: parameterization of the SWRC according to the BC–based version of Fayers and Simmons (1995)

RIA: parameterization of the SWRC that combines RNA and VGA

RNA: parameterization of the SWRC according to the junction model of Rossi and Nimmo (1994)

SWRC: soil water retention curve

RMSE: root mean square error

UNSODA: unsaturated soil hydraulic properties database

VGA: parameterization of the SWRC according to Ippisch et al. (2016)

VGN: parameterization of the SWRC according to the original van Genuchten (1980) equation

https://doi.org/10.5194/hess-2020-380
Preprint. Discussion started: 17 August 2020

Hydrology and Earth System Sciences
Discussions
Open Access
EGU

Appendix B. Assessing the near-saturation behavior of recently developed soil water retention and hydraulic conductivity curves

Madi et al. (2018) developed a criterion that needs to be met to avoid unphysical behavior of the unsaturated soil hydraulic conductivity curve near saturation:

$$\lim_{h\uparrow 0}\left(|h|^{-\kappa}\frac{\mathrm{d}\theta}{\mathrm{d}h}\right)=0 \tag{B1}$$

where κ is a fitting parameter (>0) that appears in a several parameterizations of the unsaturated soil hydraulic conductivity curve based on the capillary bundle conceptualization.

Fredlund and Xing (1994) introduced the following parameterization for the soil water retention curve:

$$\theta(h)=\left[\frac{-\ln\left(1+\frac{|h|}{|h_\mathrm{r}|}\right)}{\ln\left(1+\frac{b}{|h_\mathrm{r}|}\right)}+1\right]\frac{\theta_\mathrm{s}}{\left\{\ln\left[\mathrm{e}+\left(\frac{|h|}{a}\right)^{n}\right]\right\}^{m}} \tag{B2}$$

where the subscript 'r' denotes the value when the residual water content is reached, and a [L], n, and m are fitting parameters. The first term on the right-hand side is a correction term that forces the water content to zero for $h=-b$, with b equal to 10^7 cm (Fredlund and Xing, 1994) or 6.3×10^6 cm (Wang et al., 2016). Wang et al. (2016) also modified the correction factor to give

https://doi.org/10.5194/hess-2020-380
Preprint. Discussion started: 17 August 2020


Hydrology and Earth System Sciences
Discussions
Open Access
EGU

$$\theta(h) = \left[\frac{-\ln\left(1+\frac{c|h|}{|h_r|}\right)}{\ln\left(1+\frac{bc}{|h_r|}\right)} + 1\right]\frac{\theta_s}{\left\{\ln\left[e+\left(\frac{|h|}{a}\right)^n\right]\right\}^m} \quad \text{(B3)}$$

where c has to be small and positive. The derivative of Eq. (B3) is

$$\frac{d\theta}{dh} = \frac{-\theta_s}{\left\{\ln\left[e+\left(\frac{|h|}{a}\right)^n\right]\right\}^m}\left\{\frac{mn|h|^{n-1}\left[\ln\left(1+\frac{bc}{|h_r|}\right)\ln\left(1+\frac{c|h|}{|h_r|}\right)-1\right]}{a^n\left[e+\left(\frac{|h|}{a}\right)^n\right]\ln\left[e+\left(\frac{|h|}{a}\right)^n\right]} - \frac{\ln\left(1+\frac{bc}{|h_r|}\right)}{\frac{|h_r|}{c}+|h|}\right\} \quad \text{(B4)}$$

The derivative of Eq. (B2) follows by setting c equal to 1 in Eq. (B4). Combining Eq.(B4) with Eq. (B1) results in the following requirement:

$$\lim_{h\uparrow 0}\left[\frac{\theta_s mn}{ea^n}|h|^{-\kappa+n-1} + \frac{c\theta_s\ln\left(1+\frac{bc}{|h_r|}\right)}{|h_r|}|h|^{-\kappa}\right]=0 \quad \text{(B5)}$$

The limit goes to zero if and only if the exponents of in both terms are positive. Hence, $\kappa < n-1$ and $\kappa < 0$. The first requirement may be met for some soils, but the second violates the physical constraint that κ cannot be negative (Madi et al., 2018). Therefore, neither Fredlund and Xing's (1994) nor Wang et al.'s (2016) parameterization lead to unsaturated hydraulic conductivity curves that exhibit physically realistic behavior near saturation. Wang et al. (2018) added a modification in the dry end of Wang et al. (2016), and Rudiyanto et al. (2020) in turn used Wang et al.'s (2018) curves. Because the problem near saturation was not resolved, these two hydraulic conductivity models suffer from the same problem near saturation.

https://doi.org/10.5194/hess-2020-380
Preprint. Discussion started: 17 August 2020


Hydrology and Earth System Sciences
Discussions

Appendix C. Fitted Parameters and Root Mean Square Error for Six Parameterizations of the Soil Water Retention Curve applied to Data of 21 Soils

The UNSODA soils selected for parameter fitting are grouped in Tables C1–C4 according to their texture classification according to Twarakavi et al. (2010). Sand is a major constituent of the mineral soil in Tables C1 and C2, silt in Table C3, and clay in Table C4. Figure C1 shows the textural composition of the soils. For each soil, the parameter values for six parameterizations are given, resulting in a total of 126 SWRC parameterizations. The Root Mean Square Errors (RMSE) for all fits are listed in Tables C5–C8. The saturated hydraulic conductivities of the soils as given by the UNSODA database are given in Table C9.

Madi et al. (2018) provide an analysis of the underlying functions of all parameterizations tested here, except RIA. The meaning of all variables except λ is explained in the main text. Variable λ is the power to which the factor (h / h_{ae}) is raised in the power–law segments of the SWRCs of BCO, FSB, and RNA. In RNA, λ is expressed as a function of the fitting parameters, and therefore does not appear in the tables.

The SWRCs defined by these parameterizations together with the data points on which they are based are given in Figs. C2–C5. The hydraulic conductivity curves according to Mualem (1976) that can be derived from the parameterizations (Eqs. (13a) and (13b) for RIA, equations for the other parameterizations in Madi et al. (2018)) are plotted in Figs. C6–C9. We plotted K as a function of θ because this relationship is less hysteretic than $K(h)$

https://doi.org/10.5194/hess-2020-380
Preprint. Discussion started: 17 August 2020


Hydrology and Earth System Sciences
Discussions

(Koorevaar et al., 1983, p. 141) and some of the UNSODA data only provided $K(\theta)$ data points. The conductivity data available in UNSODA are also plotted, but these were not used to fit the curves to.

The comparison of theoretical conductivity curves based on water retention data with the measured values showed a sometimes substantial deviation between hydraulic conductivities measured at saturation and the K_s value used to create the theoretical curves. The latter value was obtained by a query that made the database return a K_s value for the soils that met all other criteria also included in the query. The conductivity data displayed in the plots were separately obtained by requesting the database to return a report of tabular data for each of the 21 soils. The reasons for the discrepancies between the queried value and the tabulated may reflect separate experiments for measuring unsaturated and saturated values of K.

There also are obvious differences between the water content at saturation between the retention and the conductivity data. In all but one case (soil 4450, Fig. C8) the hydraulic conductivity observations were made in the field whereas the retention data used were all obtained from drying experiments in the laboratory. Scale differences, effects of air enclosure and hysteresis in the field, and differences between different measurement techniques explain these differences. We can therefore only compare the shape of the theoretical curves with those of the data clouds.

https://doi.org/10.5194/hess-2020-380
Preprint. Discussion started: 17 August 2020

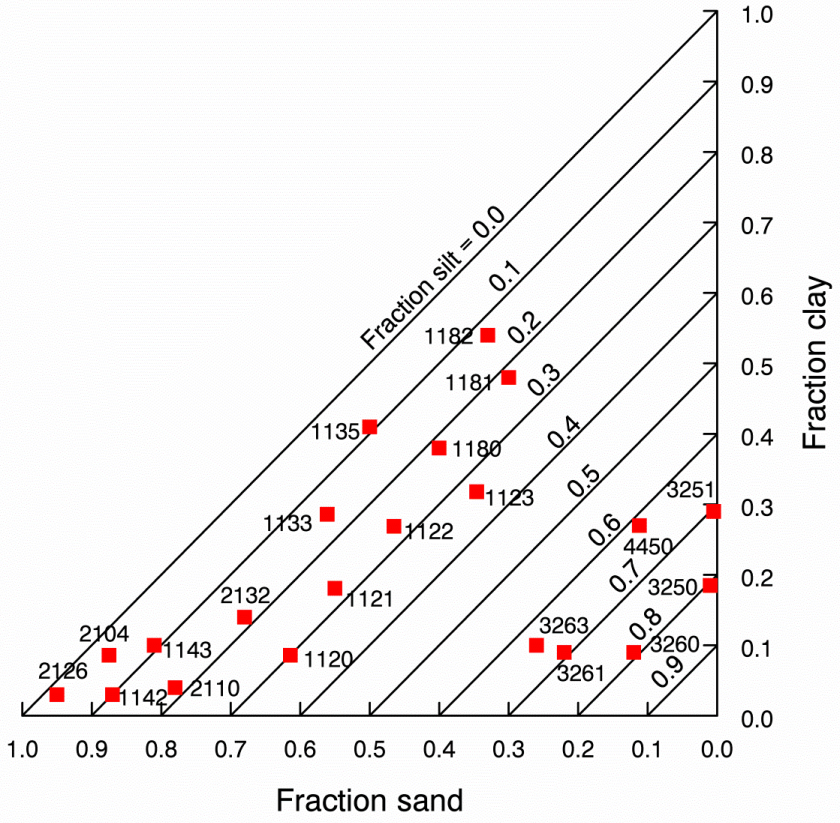

Figure C1. The positions in the texture triangle of the selected soils, indicated by their UNSODA identifier. (Taken form Madi et al., 2018)

https://doi.org/10.5194/hess-2020-380
Preprint. Discussion started: 17 August 2020


Hydrology and Earth System Sciences
Discussions

493 The RMSE was calculated from the weighted sum of squares of the differences
494 between calculated and observed water contents and pressure heads. The weights equaled
495 the estimated scaled standard deviations of the individual water retention observations
496 (pairs of matric potential and water content values). The standard deviations of the water
497 content observations were scaled to have an average value of 0.2. The scale factor needed to
498 arrive at this value was then applied to the standard deviations of the matric potential
499 values as well. This ensured that the weighting of water contents and matric potential
500 values was consistent with the original standard deviations of both. The scaling greatly
501 improved the efficiency of the parameter fitting procedure. The squared difference between
502 a single observed water content and its fitted value during a given iteration of the
503 parameter fitting algorithm, taking into account observation errors in both the water
504 content and the matric potential, is
505
506 $$\left(\frac{\theta_{\mathrm{fit}}-\theta_{\mathrm{obs}}}{\sigma_{\theta,\,\mathrm{scaled}}+\sigma_{h,\mathrm{scaled}}\frac{d\theta}{dh}\Big|_{h_{\mathrm{obs}}}}\right)^2 \qquad \text{(C1)}$$

507
508 where $\sigma_{a,\,\mathrm{scaled}}$ is the scaled standard deviation of the variable a, subscript 'fit' signifies a
509 fitted value of the subscripted variable, and subscript 'obs' a measured value (Madi et al.,
510 2018). The slope of the SWRC in the denominator is estimated from the fitted
511 parameterization using the parameter values that have been fitted in the iteration that is
512 currently being tested.
513 The scale factors applied to the observation error standard deviations varied
514 between soils but not between parameterizations fitted to the same soil. RMSE values of

https://doi.org/10.5194/hess-2020-380
Preprint. Discussion started: 17 August 2020


Hydrology and Earth System Sciences
Discussions

different parameterizations valid for a particular soil can therefore be readily compared. Comparisons between soils only give a rough indication. When the water contents at which measurements were taken differ strongly from one soil to another, the comparison of their RMSE values is less reliable.

In case the measured water contents were obtained at hydrostatic equilibrium, the fitted water content calculated directly from the matric potential could not be compared to the observed water content. To approximate the soil sample on which the observation was made, a hypothetical soil slab of the same height as the sample was divided into 20 horizontal layers. If UNSODA did not specify the sample height, it was assumed to be 5.0 cm. The matric potential in the center of each layer was determined from the given matric potential, which was assumed to apply to the center of the sample. The water content of the soil slab was then calculated as the average water content of its 20 layers. This water content was used to calculate the difference between the observed and the fitted water content. Figure C10 shows a comparison of retention points calculated for three soils based directly on the RIA parameterization and based on the same parameterization applied to a hypothetical sample of 5.0 cm height at hydrostatic equilibrium with the nominal matric potential valid at the sample center. Deviations are small, even for the loamy sand.

https://doi.org/10.5194/hess-2020-380
Preprint. Discussion started: 17 August 2020

532 Table C1. The fitting parameters and their values for six parameterizations for sandy soils in the A1
533 and A2 classifications of Twarakavi et al. (2010) from the UNSODA database (National Agricultural
534 Library, 2017; Nemes et al., 2001). The three–character parameterization label is explained in the
535 main text.

			Soil (UNSODA identifier and classification according to Twarakavi et al. (2010))		
			2126 A1	1142 A2	2104 A2
Parameterization	Parameter	Unit			
BCO	θ_r	–	1.63E–2	4.92E–5	2.27E–2
	θ_s	–	0.377	0.250	0.398
	h_{ae}	cm	–6.78	–7.00	–6.79
	λ	–	0.846	0.210	0.434
FSB	θ_s	–	0.377	0.250	0.398
	θ_a	–	2.58E–2	6.26E–5	5.46E–2
	h_{ae}	cm	–6.76	–7.00	–6.73
	λ	–	0.861	0.211	0.468
RNA	θ_s	–	0.378	0.250	0.398
	h_{ae}	cm	–6.37	–7.00	–6.17
	h_j	cm	–8.87E4	–9.24E4	–6.45E4
	h_d	cm	–3.60E5	–1.07E7	–9.73E5
VGN	θ_r	–	3.39E–2	9.42E–2	3.41E–2
	θ_s	–	0.376	0.242	0.398
	α	cm^{-1}	6.85E–2	1.99E–2	6.97E–2
	n	–	2.73	2.93	1.64
VGA	θ_r	–	3.39E–2	9.64E–2	3.42E–2
	θ_s	–	0.376	0.242	0.398
	α	cm^{-1}	6.84E–2	1.98E–2	6.97E–2
	n	–	2.73	3.05	1.64
	h_{ae}	cm	–0.101	–0.240	–1.62E–2
RIA	θ_s	–	0.378	0.245	0.398
	α	cm^{-1}	0.239	2.68E–2	0.171
	n	–	1.77	1.47	1.41
	h_{ae}	cm	–5.82	–7.00	–4.36
	h_j	cm	–1.76E6	–4.35E5	–7.75E5

536

https://doi.org/10.5194/hess-2020-380
Preprint. Discussion started: 17 August 2020

Hydrology and Earth System Sciences
Discussions

537 Table C2. The fitting parameters and their values for six parameterizations for sandy soils in the A3
538 and A4 classifications of Twarakavi et al. (2010) from the UNSODA database (National Agricultural
539 Library, 2017; Nemes et al., 2001). The three–character parameterization label is explained in the
540 main text.

			Soil (UNSODA identifier and classification according to Twarakavi et al. (2010))					
			1120 A3	1143 A3	2110 A3	2132 A3	1121 A4	1133 A4
Para–meteri–zation	Para me–eter	Unit						
BCO	θ_r	–	6.15E–6	2.71E–5	0.103	4.10E–5	2.64E–5	5.37E–5
	θ_s	–	0.311	0.279	0.348	0.303	0.350	0.330
	h_{ae}	cm	–10.0	–7.00	–25.5	–8.00	–10.0	–206
	λ	–	0.204	0.169	0.537	0.107	0.118	0.103
FSB	θ_s	–	0.311	0.279	0.348	0.308	0.346	0.330
	θ_a	–	4.33E–5	4.26E–4	0.213	0.298	0.324	0.310
	h_{ae}	cm	–10.0	–7.00	–25.7	–3.24	–10.0	–206
	λ	–	0.204	0.169	0.763	0.422	0.377	0.213
RNA	θ_s	–	0.311	0.279	0.351	0.303	0.352	0.330
	h_{ae}	cm	–10.0	–7.00	–20.3	–8.00	–10.0	–220
	h_j	cm	–7.32E4	–8.46E4	–6.44E4	–7.18E4	–8.73E4	–6.77E4
	h_d	cm	–9.95E6	–3.18E7	–2.35E6	–8.06E8	–3.88E8	–8.68E8
VGN	θ_r	–	7.22E–2	9.24E–2	0.126	1.25E–4	1.70E–5	0.202
	θ_s	–	0.305	0.278	0.360	0.305	0.339	0.324
	α	cm^{-1}	1.72E–2	4.66E–2	2.63E–2	5.73E–2	7.21E–3	7.34E–4
	n	–	1.69	1.49	1.84	1.14	1.26	3.02
VGA	θ_r	–	7.37E–2	0.112	0.106	6.61E–4	1.47E–5	0.202
	θ_s	–	0.303	0.276	0.348	0.306	0.339	0.324
	α	cm^{-1}	1.72E–2	4.41E–2	0.230	6.06E–2	7.16E–3	7.35E–4
	n	–	1.71	1.66	1.56	1.14	1.27	3.00
	h_{ae}	cm	–9.37	–6.81	–25.3	–8.47E–4	–2.73E–2	–12.5
RIA	θ_s	–	0.308	0.280	0.360	0.306	0.339	0.328
	α	cm^{-1}	3.01E–2	6.39E–2	4.18E–2	6.08E–2	7.13E–2	1.30E–3
	n	–	1.29	1.23	1.33	1.14	1.27	1.20
	h_{ae}	cm	–1.24E–3	–4.96E–4	–7.85	–7.44E–4	–9.11E–4	–220
	h_j	cm	–1.71E6	–7.01E6	–9.37E6	–7.81E6	–2.04E6	–5.07E6

https://doi.org/10.5194/hess-2020-380
Preprint. Discussion started: 17 August 2020

Hydrology and Earth System Sciences
Discussions

Table C3. The fitting parameters and their values for six parameterizations for silty soils from the UNSODA database (National Agricultural Library, 2017; Nemes et al., 2001). The three–character parameterization label is explained in the main text.

			Soil (UNSODA identifier and classification according to Twarakavi et al. (2010))					
			3260 B2	3261 B2	3263 B2	3250 B4	3251 B4	4450 B4
Para–meteri–zation	Para me–ter	Unit						
BCO	θ_r	–	2.85E–6	3.42E–6	3.85E–7	3.85E–6	1.94E–6	2.77E–5
	θ_s	–	0.470	0.499	0.460	0.540	0.500	0.380
	h_{ae}	cm	–28.6	–13.5	–28.8	–30.5	–18.2	–4.80
	λ	–	0.281	0.256	0.255	0.183	9.56E–2	9.51E–2
FSB	θ_s	–	0.470	0.499	0.460	0.540	0.500	0.380
	θ_a	–	1.33E–5	6.49E–5	1.33E–5	0.173	0.431	0.320
	h_{ae}	cm	–28.6	–13.5	–28.8	–30.0	–10.9	–0.882
	λ	–	0.281	0.256	0.255	0.241	0.197	0.196
RNA	θ_s	–	0.470	0.499	0.460	0.540	0.500	0.380
	h_{ae}	cm	–28.6	–13.5	–28.8	–30.5	–18.2	–4.81
	h_j	cm	–9.23E4	–9.43E4	–7.48E4	–7.87E4	–1.97E4	–2.63E4
	h_d	cm	–3.23E6	–4.96E6	–3.75E6	–6.86E6	–7.66E8	–9.69E8
VGN	θ_r	–	5.25E–2	4.88E–2	4.48E–2	3.10E–2	1.60E–5	1.16E–6
	θ_s	–	0.472	0.491	0.461	0.540	0.501	0.379
	α	cm^{-1}	1.62E–2	1.84E–2	1.53E–2	1.21E–2	2.62E–2	0.164
	n	–	1.47	1.51	1.41	1.28	1.11	1.10
VGA	θ_r	–	5.27E–2	4.89E–2	6.12E–2	3.80E–4	7.21E–5	2.80E–5
	θ_s	–	0.472	0.491	0.457	0.540	0.500	0.379
	α	cm^{-1}	1.62E–2	1.84E–2	1.49E–2	1.33E–2	3.66E–2	1.26
	n	–	1.47	1.52	1.46	1.25	1.11	1.10
	h_{ae}	cm	–3.26E–3	–2.08E–3	–15.1	–4.87	–7.31	–4.54
RIA	θ_s	–	0.474	0.493	0.463	0.540	0.500	0.379
	α	cm^{-1}	2.04E–2	2.33E–2	1.86E–2	1.33E–2	3.57E–2	0.164
	n	–	1.33	1.37	1.31	1.25	1.11	1.10
	h_{ae}	cm	–5.95E–3	–2.36E–3	–2.43E–3	–4.80	–7.12	–1.21E–3
	h_j	cm	–1.49E6	–1.07E6	–8.62E6	–8.02E6	–8.33E6	–9.89E6

https://doi.org/10.5194/hess-2020-380
Preprint. Discussion started: 17 August 2020

Hydrology and Earth System Sciences
Discussions

545 Table C4. The fitting parameters and their values for six parameterizations for clayey soils from the
546 UNSODA database (National Agricultural Library, 2017; Nemes et al., 2001). The three–character
547 parameterization label is explained in the main text.

			Soil (UNSODA identifier and classification according to Twarakavi et al. (2010))					
			1135 C2	1182 C2	1122 C4	1123 C4	1180 C4	1181 C4
Para–meteri–zation	Para–meter	Unit						
BCO	θ_r	–	3.94E–4	1.79E–4	2.64E–4	2.13E–4	5.22E–4	1.24E–5
	θ_s	–	0.420	0.549	0.362	0.358	0.497	0.456
	h_{ae}	cm	–106	–0.977	–10.0	–10.0	–11.1	–5.17
	λ	–	7.85E–2	4.41E–2	3.37E–2	2.69E–2	5.65E–2	5.40E–2
FSB	θ_s	–	0.420	0.548	0.360	0.356	0.495	0.456
	θ_a	–	0.400	0.307	0.350	0.340	0.491	0.345
	h_{ae}	cm	–106	–0.230	–5.75	–10.0	–8.58	–13.2
	λ	–	0.172	5.64E–2	6.60E–2	5.69E–2	100	8.08E–2
RNA	θ_s	–	0.420	0.549	0.370	0.370	0.497	0.456
	h_{ae}	cm	–106	–3.61	–9.99	–9.99	–0.150	–7.66
	h_j	cm	–107	–12.2	–10.5	–10.7	–24.1	–22.1
	h_d	cm	–1.64E8	–1.00E9	–1.00E9	–1.00E9	–1.00E9	–1.00E9
VGN	θ_r	–	0.263	8.94E–6	1.16E–4	0.210	0.255	3.34E–6
	θ_s	–	0.413	0.548	0.359	0.354	0.496	0.456
	α	cm^{-1}	1.02E–3	0.753	1.37E–2	2.92E–3	0.805	0.143
	n	–	2.37	1.05	1.05	1.21	1.26	1.06
VGA	θ_r	–	0.263	1.19E–5	5.78E–2	0.188	2.63E–2	2.12E–6
	θ_s	–	0.413	0.548	0.359	0.354	0.498	0.456
	α	cm^{-1}	1.02E–3	1.21	1.37E–2	3.22E–3	10.1	1.70
	n	–	2.37	1.05	1.07	1.17	1.06	1.05
	h_{ae}	cm	–1.03	–0.467	–4.18E–2	–10.0	–1.11E–2	–4.83
RIA	θ_s	–	0.416	0.548	0.359	0.354	0.497	0.457
	α	cm^{-1}	1.86E–3	1.31	1.39E–2	4.00E–3	14.2	0.702
	n	–	1.16	1.05	1.05	1.06	1.06	1.05
	h_{ae}	cm	–106	–0.525	–3.80E–3	–9.99	–4.41E–2	–4.25
	h_j	cm	–7.57E6	–9.97E6	–9.56E4	–4.43E6	–415	–206

548

https://doi.org/10.5194/hess-2020-380
Preprint. Discussion started: 17 August 2020

Hydrology and Earth System Sciences
Discussions

549 Table C5. Root mean square errors of the parameter fits for the sandy or loamy soils (A1 and A2
550 soils according to Twarakavi et al., 2010)

	Soil (UNSODA identifier and classification according to Twarakavi et al. (2010))		
Parameterization	2126 A1	1142 A2	2104 A2
BCO	0.0620	0.0990	0.0481
FSB	0.0626	0.0990	0.0517
RNA	0.0659	0.0989	0.0553
VGN	0.0330	0.0252	0.0278
VGA	0.0330	0.0250	0.0278
RIA	0.0652	0.0504	0.0542

551

552

https://doi.org/10.5194/hess-2020-380
Preprint. Discussion started: 17 August 2020

553 Table C6. Root mean square errors of the parameter fits for the sandy soils (A3 and A4 soils
554 according to Twarakavi et al., 2010)

Parameterization	Soil (UNSODA identifier and classification according to Twarakavi et al. (2010))					
	1120 A3	1143 A3	2110 A3	2132 A3	1121 A4	1133 A4
BCO	0.0926	0.0501	0.0445	0.0356	0.1288	0.0803
FSB	0.0926	0.0500	0.0445	0.0292	0.1054	0.0700
RNA	0.0926	0.0500	0.0457	0.0356	0.1286	0.0775
VGN	0.0446	0.0333	0.0378	0.0204	0.0720	0.0175
VGA	0.0489	0.0396	0.0445	0.0203	0.0720	0.0175
RIA	0.0643	0.0346	0.0491	0.0203	0.0720	0.0530

555

556

https://doi.org/10.5194/hess-2020-380
Preprint. Discussion started: 17 August 2020

557 Table C7. Root mean square errors of the parameter fits for the silty soils.

	Soil (UNSODA identifier and classification according to Twarakavi et al. (2010))					
Parameterization	3260 B2	3261 B2	3263 B2	3250 B4	3251 B4	4450 B4
BCO	0.0793	0.1316	0.0973	0.0822	0.0551	0.0499
FSB	0.0794	0.1316	0.0973	0.0815	0.0395	0.0445
RNA	0.0793	0.1316	0.0973	0.0822	0.0551	0.0499
VGN	0.0456	0.0607	0.0638	0.0413	0.0474	0.0485
VGA	0.0455	0.0607	0.0769	0.0412	0.0466	0.0497
RIA	0.0543	0.0698	0.0668	0.0412	0.0466	0.0485

558

559

https://doi.org/10.5194/hess-2020-380
Preprint. Discussion started: 17 August 2020


Hydrology and Earth System Sciences
Discussions

560 Table C8. Root mean square errors of the parameter fits for the clayey soils.

Parameterization	Soil (UNSODA identifier and classification according to Twarakavi et al. (2010))					
	1135 C2	1182 C2	1122 C4	1123 C4	1180 C4	1181 C4
BCO	0.0913	0.0494	0.0349	0.0489	0.0187	0.0428
FSB	0.0721	0.0441	0.0212	0.0321	0.1196	0.0360
RNA	0.0812	0.0913	0.1235	0.1501	0.0347	0.0570
VGN	0.0208	0.0488	0.0197	0.0244	0.0411	0.0433
VGA	0.0208	0.0485	0.0198	0.0243	0.0197	0.0429
RIA	0.0519	0.0485	0.0197	0.0244	0.0180	0.0391

561

562

https://doi.org/10.5194/hess-2020-380
Preprint. Discussion started: 17 August 2020


Hydrology and Earth System Sciences
Discussions

563 Table C9. Values for the hydraulic conductivity at saturation (K_s) for the selected soils from
564 the UNSODA database. The soils are identified by their UNSODA identifier. Their classification
565 according to Twarakavi et al. (2010) is also given.

UNSODA identifier	Texture classification	K_s (cm d^{-1})
2126	A1	1.10E3
1142	A2	13.4
2104	A2	553
1120	A3	37.9
1143	A3	23.5
2110	A3	16.3
2132	A3	5.52
1121	A4	7.13
1133	A4	7.13
3260	B2	10.8
3261	B2	32.0
3263	B2	54.0
3250	B4	1.51
3251	B4	2.74
4450	B4	1.20
1135	C2	0.142
1182	C2	1.25
1122	C4	2.92
1123	C4	0.740
1180	C4	215
1181	C4	178

566

https://doi.org/10.5194/hess-2020-380
Preprint. Discussion started: 17 August 2020

Hydrology and Earth System Sciences
Discussions
Open Access
EGU

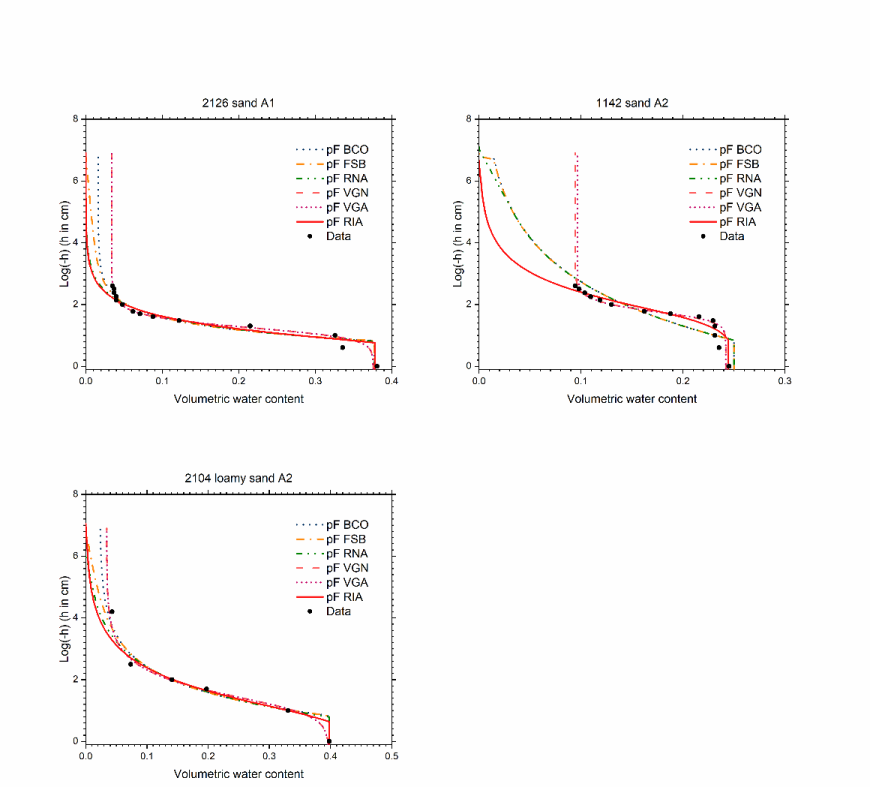

Figure C2. Retention data and fitted soil water retention curves according to six parameterizations for selected UNSODA soils with Twarakavi et al.'s (2010) A1 or A2 classification. The parameterizations are explained in the text.

https://doi.org/10.5194/hess-2020-380
Preprint. Discussion started: 17 August 2020

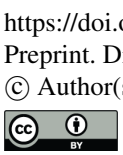

Hydrology and Earth System Sciences
Discussions
Open Access
EGU

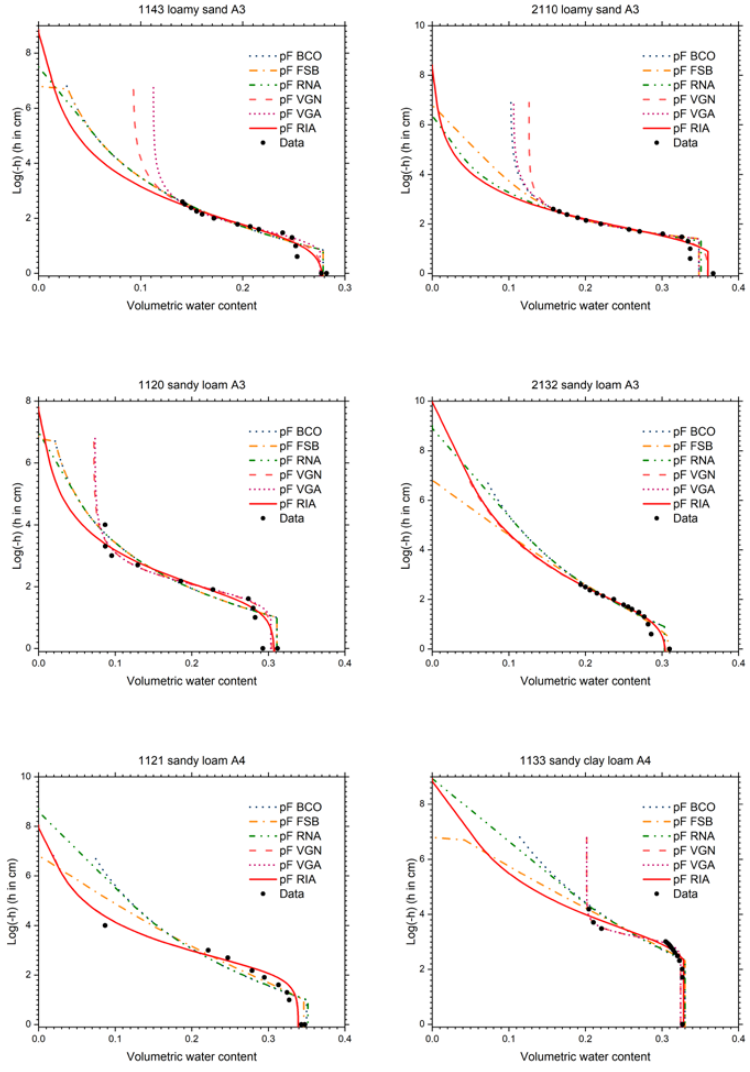

571

572 Figure C3. Retention data and fitted soil water retention curves according to six

573 parameterizations for selected UNSODA soils with Twarakavi et al.'s (2010) A3 or A4

574 classification. The parameterizations are explained in the text.

https://doi.org/10.5194/hess-2020-380
Preprint. Discussion started: 17 August 2020

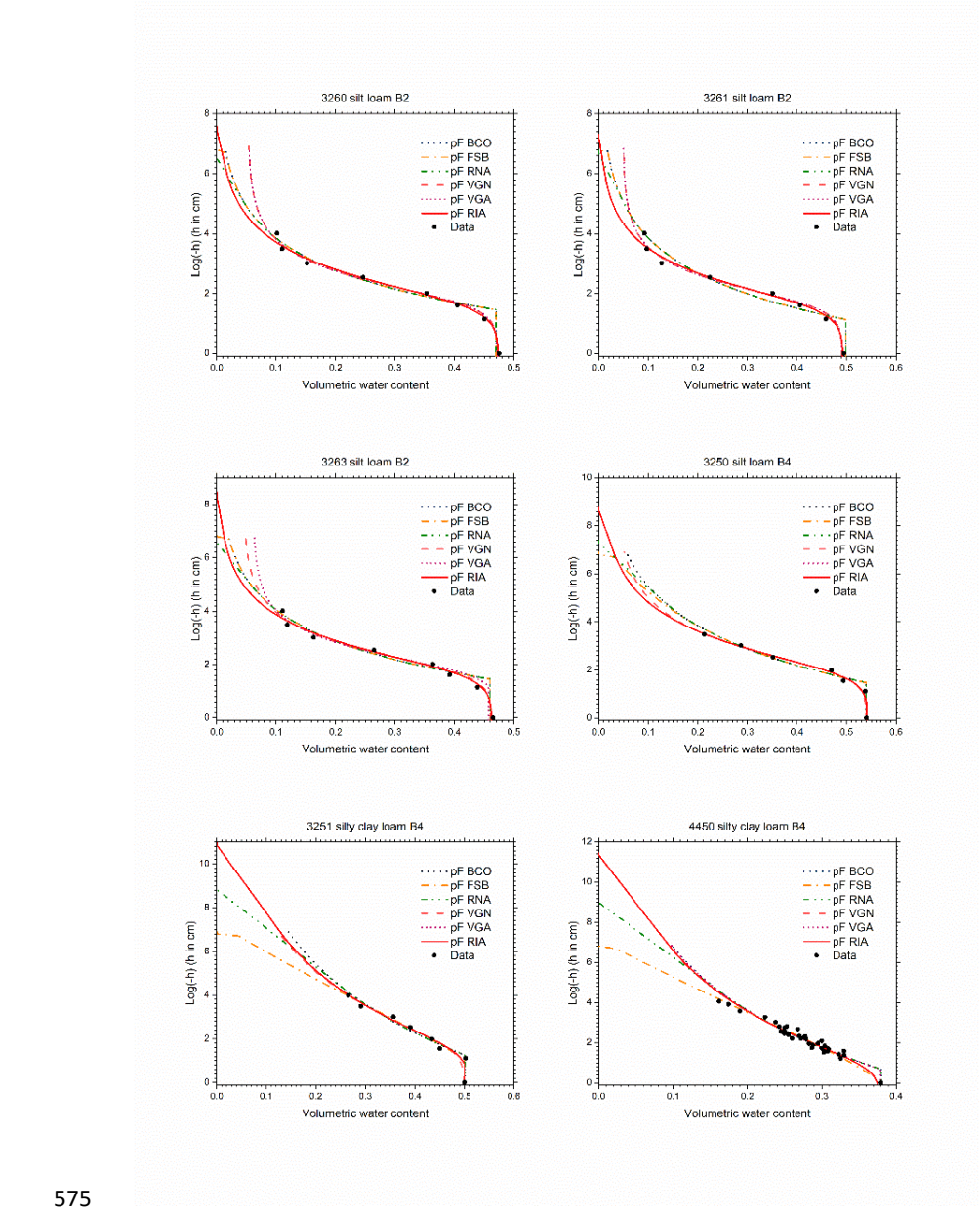

575

576 Figure C4. Retention data and fitted soil water retention curves according to six

577 parameterizations for selected UNSODA soils with Twarakavi et al.'s (2010) B2 or B4

578 classification. The parameterizations are explained in the text.

https://doi.org/10.5194/hess-2020-380
Preprint. Discussion started: 17 August 2020

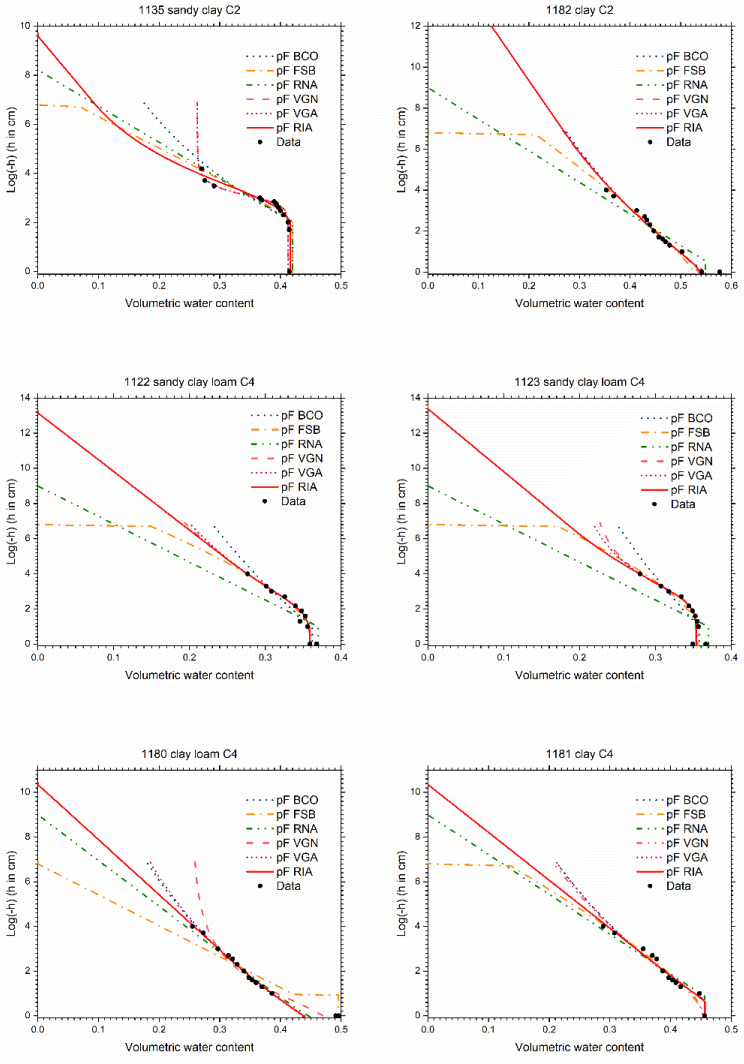

579

580 Figure C5. Retention data and fitted soil water retention curves according to six
581 parameterizations for selected UNSODA soils with Twarakavi et al.'s (2010) C2 or C4
582 classification. The parameterizations are explained in the text.

https://doi.org/10.5194/hess-2020-380
Preprint. Discussion started: 17 August 2020

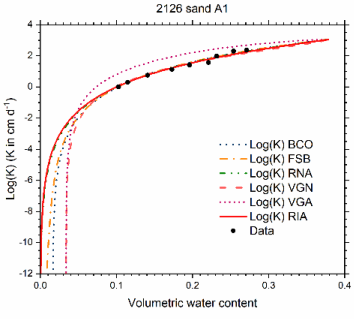

Hydrology and Earth System Sciences
Discussions
Open Access
EGU

583

584 Figure C6. Conductivity data and conductivity curves derived from the retention curves of

585 Fig. C2 according to six parameterizations for selected UNSODA soils with Twarakavi et al.'s

586 (2010) A1 or A2 classification.

https://doi.org/10.5194/hess-2020-380
Preprint. Discussion started: 17 August 2020

Hydrology and Earth System Sciences
Discussions
Open Access
EGU

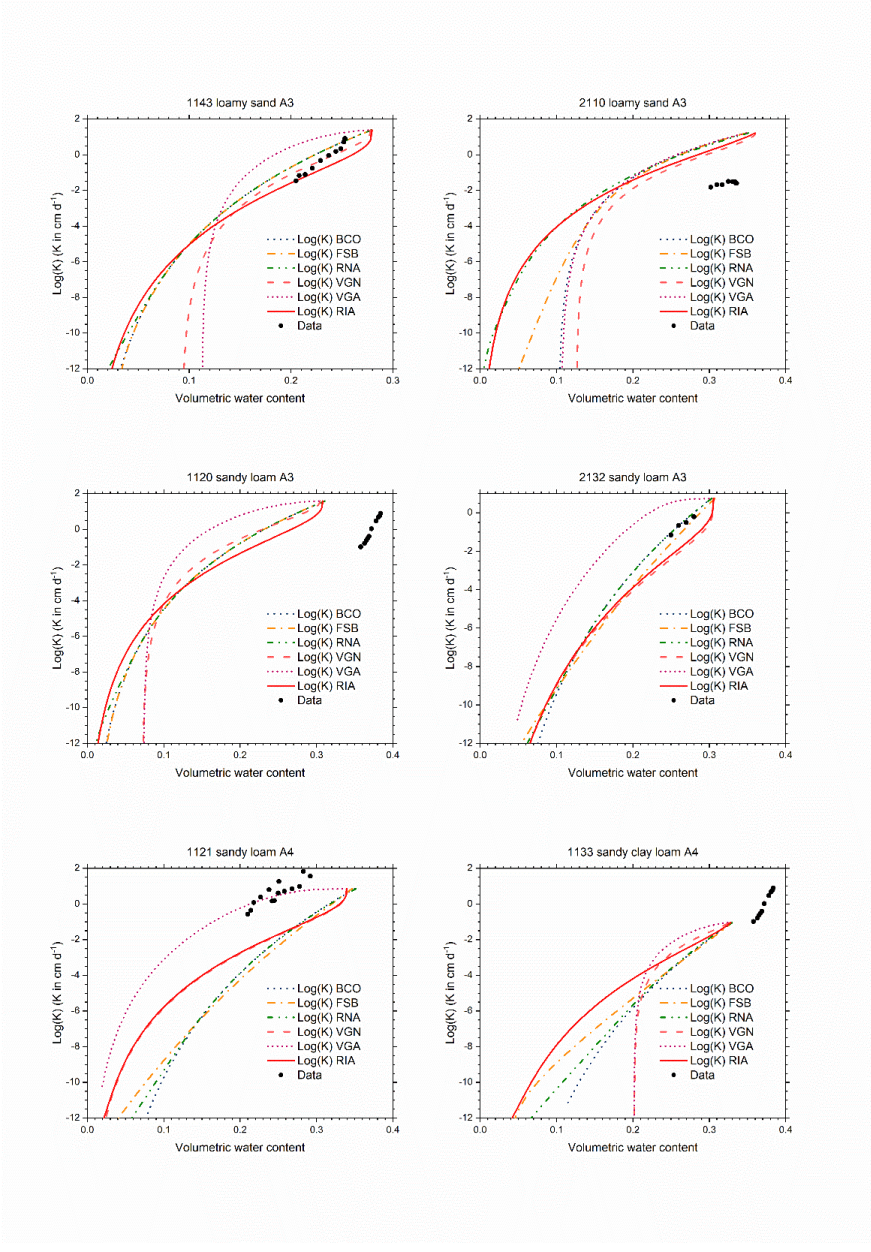

587

588 Figure C7. Conductivity data and conductivity curves derived from the retention curves of
589 Fig. C3 according to six parameterizations for selected UNSODA soils with Twarakavi et al.'s
590 (2010) A3 or A4 classification.

https://doi.org/10.5194/hess-2020-380
Preprint. Discussion started: 17 August 2020

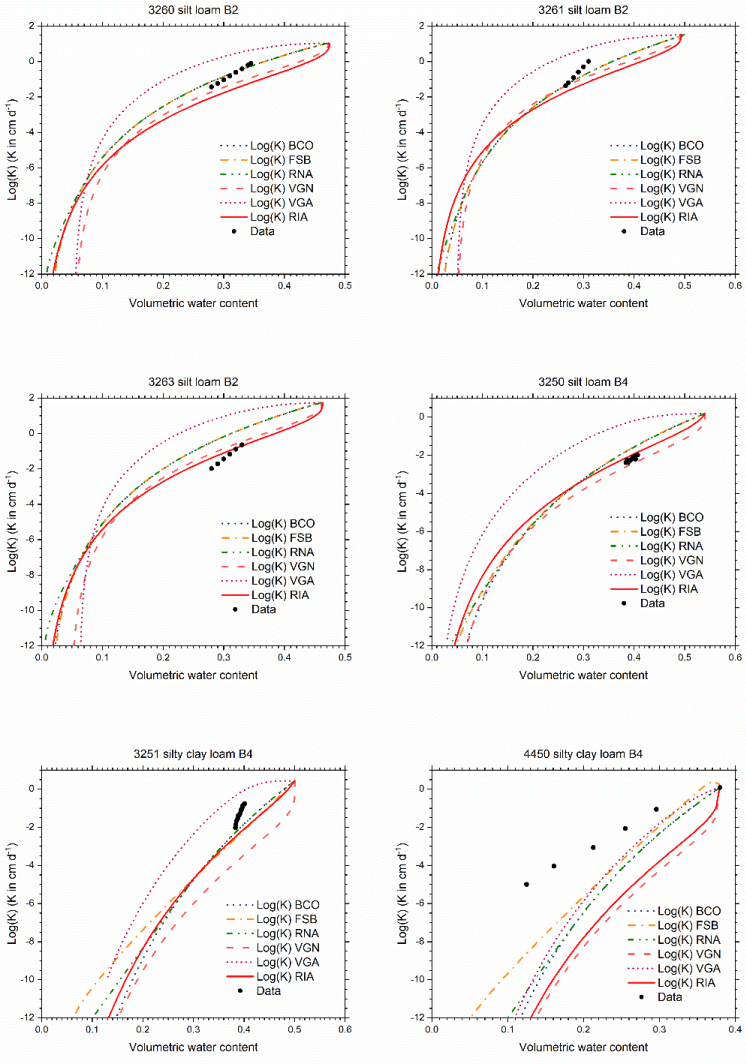

591

592 Figure C8. Conductivity data and conductivity curves derived from the retention curves of
593 Fig. C4 according to six parameterizations for selected UNSODA soils with Twarakavi et al.'s
594 (2010) B2 or B4 classification.

https://doi.org/10.5194/hess-2020-380
Preprint. Discussion started: 17 August 2020

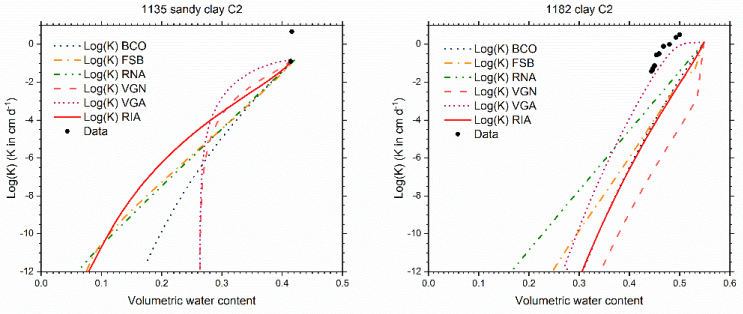

Hydrology and Earth System Sciences
Discussions

595

596 Figure C9. Conductivity data and conductivity curves derived from the retention curves of

597 Fig. C5 according to six parameterizations for selected UNSODA soils with Twarakavi et al.'s

598 (2010) C2 or AC4 classification.

https://doi.org/10.5194/hess-2020-380
Preprint. Discussion started: 17 August 2020

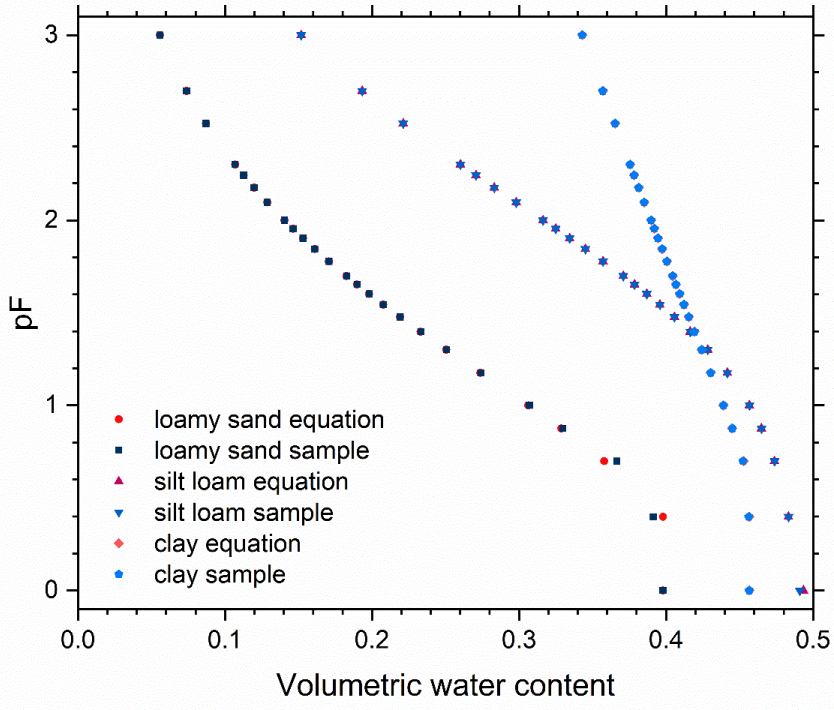

Figure C10. Soil water retention points calculated from RIA parameterizations for loamy sand (UNSODA identifier 2104, classification according to Twarakavi et al. (2010) A4), silt loam (3261, B2), and clay (1181, C4). The points were either calculated directly for the given pF value ('equation'), or by calculating the average water content in a sample of 5.0 cm height at hydrostatic equilibrium, with the matric potential at the center of the sample corresponding to the indicated pF value ('sample'). N.B. The data points for zero matric potential were plotted at pF = 0 instead of pF = $-\infty$.

https://doi.org/10.5194/hess-2020-380
Preprint. Discussion started: 17 August 2020

Author contributions

GdR developed the new parameterization, assisted by RM. GdR identified the 21 soils from the UNSODA database and designed the model test. JM developed the SCE code for parameter identification. GdR coded the shell around the SCE core to make it suitable for fitting various SWRC parameterizations. GdR collected the weather data and generated the weather records. GdR and RM carried out the paramter fitting and the Hydrus–1D simulations. GdR wrote the manuscript with contributions from JM and RM.

Competing interests

GdR is a member of the HESS Editorial Board.

https://doi.org/10.5194/hess-2020-380
Preprint. Discussion started: 17 August 2020


Hydrology and Earth System Sciences
Discussions

620 # References

621 Assouline, S., and Or, D.: Conceptual and parametric representation of soil hydraulic
622 properties: a review, Vadose Zone J., doi: 10.2136/vzj2013.07.0121, 2013.
623 Assouline, S., Tessier, D., and Bruand, A.: A conceptual model of the soil water retention
624 curve, Water Resour. Res., 34, 223–231, 1998.
625 Bittelli, M., and Flury, M.: Errors in water retention curves determined with pressure plates,
626 Soil Sci. Soc. Am. J., 73, 1453–1460, doi: 10.2136/sssaj2008.0082, 2009.
627 Bradley, R. S.: Polymolecular adsorbed films. Part 1. The adsorption of argon on salt crystals
628 at low temperatures, and the determination of surface fields, J. Chem. Soc.
629 (Resumed), 1467–1474, doi: 10.1039/JR9360001467, 1936.
630 Brooks, R. H., and Corey, A. T.: Hydraulic properties of porous media, Hydrology Paper No.
631 3, Colorado State University, 1964.
632 Campbell, G. S., and Shiozawa, S.: Prediction of hydraulic properties of soils using particle–
633 size distribution and bulk density data, in: Proceedings of the international
634 workshop on indirect methods for estimating the hydraulic properties of
635 unsaturated soils, Riverside, California, Oct. 11–13, 1989, edited by: van Genuchten,
636 M. Th., Leij, F. J., and Lund, L. J.editors, Univ. California, Riverside, CA, U.S.A., 317–
637 328, 1992.
638 Cornelis, W. M., Khlosi, M., Hartmann, R., Van Meirvenne, M., and De Vos, B.: Comparison of
639 unimodal analytical expressions for the soil–water retention curve, Soil Sci. Soc. Am.
640 J. 69, 1902–1911, doi: 10.2136/sssaj2004.0238, 2005.
641 Durner, W.: Hydraulic conductivity estimation for soils with heterogeneous pore structure,
642 Water Resour. Res., 30, 211–223, 1994.

https://doi.org/10.5194/hess-2020-380
Preprint. Discussion started: 17 August 2020

643 Fayer, M. J., and Simmons, C. S.: Modified soil water retention function for all matric
644 suctions, Water Resour. Res., 31, 1233–1238, 1995.
645 Fredlund, D. G., and Xing, A.: Equations for the soil–water characteristic curve, Can. Geotech.
646 J., 31, 521–532, 1994.
647 Fuentes, C., Haverkamp, R., Parlange, J. –Y., Brutsaert, W., Zayani, K., and Vachaud, G.:
648 Constraints on parameters in three soil–water capillary retention functions,
649 Transport in Porous Media, 6, 445–449, 1991.
650 Hillel, D.: Environmental soil physics, Academic Press, San Diego, CA, U.S.A., 1998.
651 Iden, S. C., Peters, A., and Durner, W.: Improving prediction of hydraulic conductivity by
652 constraining capillary bundle models to a maximum pore size, Adv. Water Resour.
653 85, 86–92, doi: 10.1016/j.advwatres, 2015.09.005, 2015.
654 Ippisch, O., Vogel, H. –J., and Bastian, P.: Validity limits for the van Genuchten–Mualem
655 model and implications for parameter estimation and numerical simulation, Adv.
656 Water Resour., 29, 1780–1789, doi: 10.1016/j.advwatres.2005.12.011, 2006.
657 Khlosi, M., Cornelis, W. M., Douaik, A., van Genuchten, M. Th., and Gabriels. D.: Performance
658 evaluation of models that describe the soil water retention curve between saturation
659 and oven dryness, Vadose Zone J., 7, 87–96, doi: 10.2136/vzj2007.0099, 2008.
660 Khlosi, M., Cornelis, W. M., Gabriels, D., and Sin, G.: Simple modification to describe the soil
661 water retention curve between saturation and oven dryness, Water Resour. Res., 42,
662 W11501, doi: 10.1029/2005WR004699, 2006.
663 Klute, A.: Water retention: Laboratory methods, in: Methods of soil analysis. Part 1. Physical
664 and mineralogical methods. Second edition, edited by Klute, A., American Society of

https://doi.org/10.5194/hess-2020-380
Preprint. Discussion started: 17 August 2020

Agronomy, Inc., Soil Science Society of America, Inc., Madison, WI, U.S.A., 635–662, 1986.

Kool, J. B., and Parker, J. C.: Development and evaluation of closed–form expressions for hysteretic soil hydraulic properties, Water Resour. Res., 23, 105–114, 1987.

Koorevaar, P., Menelik, G., and Dirksen, C.: Elements of soil physics, Elsevier, Amsterdam, The Netherlands, 1983.

Kosugi, K.: General model for unsaturated hydraulic conductivity for soils with lognormal pore–size distribution, Soil Sci. Soc. Am. J., 63,270–277, 1999.

Kroes, J. G., van Dam, J. C., Bartholomeus, R. P., Groenendijk, P., Heinen, M., Hendriks, R. F. A., Mulder, H. M., Supit, I., and van Walsum, P. E. V.: SWAP version 4. Theory description and user manual, Report 27480, Wageningen Environmental Research, Wageningen, The Netherlands, 244 pp, doi: 10.18174/416321, 2017.

Leij, F. J., Russell, W. B., and Lesch, S. M.: Closed–form expressions for water retention and conductivity data, Ground Water, 35, 848–858, 1997.

Liu, H. H., and Dane, J. H.: Improved computational procedure for retention relations of immiscible fluids using pressure cells, Soil Sci. Soc. Am. J., 59, 1520–1524, 1995.

Madi, R., de Rooij, G. H., Mielenz, H., and Mai, J.: Parametric soil water models: a critical evaluation of expressions for the full moisture range, Hydrol. Earth Syst. Sci. 22, 1193–1219, doi: 10.5194/hess-22-1193-2018, 2018.

Mualem, Y.: A new model for predicting the hydraulic conductivity of unsaturated porous media, Water Resour. Res., 12, 513–522, 1976.

National Agricultural Library, UNSODA Database, https://data.nal.usda.gov/dataset/unsoda-20-unsaturated-soil-hydraulic-database-

https://doi.org/10.5194/hess-2020-380
Preprint. Discussion started: 17 August 2020

688 database-and-program-indirect-methods-estimating-unsaturated-hydraulic-
689 properties_134, last access 22 July 2020.
690 Nemes, A., Schaap, M. G., Leij, F. J., and Wösten, J. H. M.: Description of the unsaturated soil
691 hydraulic database UNSODA version 2.0., J. Hydrol., 251, 152–162, doi:
692 10.1016/S0022-1694(01)00465-6, 2001.
693 PC-progress: https://www.pc-progress.com/en/Default.aspx?hydrus-1d, last access: 22
694 July 2020.
695 Peters, A.: Simple consistent models for water retention and hydraulic conductivity in the
696 complete moisture range, Water Resour. Res., 49, 6765–6780, doi:
697 10.1002/wrcr.20548, 2013.
698 Peters, A., Durner, W., and Wessolek, G.: Consistent parameter constraints for soil hydraulic
699 functions, Adv. Water Resour., 34, 1352–1365, doi:
700 10.1016/j.advwatres.2011.07.006, 2011.
701 Rossi, C., and Nimmo. J. R.: Modeling of soil water retention from saturation to oven
702 dryness, Water Resour. Res., 30, 701–708, 1994.
703 Rudiyanto, Minasny B., Shah, R. M., Setiawan, B. I., and van Genuchten, M. Th.: Simple
704 functions for describing soil water retention and the unsaturated hydraulic
705 conductivity from saturation to complete dryness, J. Hydrol., 588, 125041, doi:
706 10.1016/j.jhydrol.2020.125041, 2020.
707 Schaap, M. G., and van Genuchten, M. Th.: A modified Mualem–van Genuchten formulation
708 for improved description of the hydraulic conductivity near saturation, Vadose Zone
709 J. 5, 27–34, doi: 10.2136/vzj2005.0005, 2006.

https://doi.org/10.5194/hess-2020-380
Preprint. Discussion started: 17 August 2020

710 Schneider, M, and Goss, K. –U.: Prediction of the water sorption isotherm in air dry soils,
711 Geoderma, 170, 64–69, doi: 10.1016/j.geoderma.2011.10.008, 2012.
712 Šimůnek, J., and Bradford, S. A.: Vadose zone modeling: Introduction and Importance,
713 Vadose Zone J., 7, 581–586, doi: 10.2136/vzj2008.0012, 2008.
714 Šimůnek, J., Šejna, M., Sait., H., Sakai, M., and van Genuchten, M. Th.: The HYDRUS–1D
715 software package for simulating the one–dimensional movement of water, heat, and
716 multiple solutes in variably–saturated media, Version 4.17, Dept. Env. Sci., Univ.
717 Calif., Riverside, CA, U.S.A., 2013.
718 Šimůnek, J, van Genuchten, M. Th., and Šejna, M.: Recent developments and applications of
719 the HYDRUS computer software packages, Vadose Zone J., doi:
720 10.2136/vzj2016.04.0033, 2016.
721 Twarakavi, N. K. C., Šimůnek, J., and Schaap, M. G.: Can texture–based classification
722 optimally classify soils with respect to soil hydraulics?, Water Resour. Res. 46,
723 W01501, doi:10.1029/2009WR007939, 2010.
724 van Genuchten, M. Th.: A closed–form equation for predicting the hydraulic conductivity for
725 unsaturated soils, Soil Sci. Soc. Am. J., 44, 892–898, 1980.
726 Vogel, T., van Genuchten, M. Th., and Cislerova, M.: Effect of the shape of the soil hydraulic
727 functions near saturation on variably–saturated flow predictions, Adv. Water
728 Resour., 24, 133–144, 2001.
729 Wang, Y., Jin, M., and Deng, Z.: Alternative model for predicting soil hydraulic conductivity
730 over the complete moisture range, Water Resour. Res., 54, 6860–6876, doi:
731 10.1029/2018WR023037, 2018.

https://doi.org/10.5194/hess-2020-380
Preprint. Discussion started: 17 August 2020


Hydrology and Earth System Sciences
Discussions

732 Wang, Y., Ma, J., and Huade, G.: A mathematically continuous model for describing the
733 hydraulic properties of unsaturated porous media over the entire range of matric
734 suctions. J. Hydrol,. 541, 873–888, doi: 10.1016/j.jhydrol.2016.07.046, 2016.
735 Weber, T. K. D., Durner, W., Streck, T., and Diamantopoulos, E.: A modular framework for
736 modeling unsaturated soil hydraulic properties over the full moisture range, Water
737 Resour. Res., 55, doi: 10.1029/2018WR024584, 2019.
738 Zurmühl, T., and Durner, W.: Determination of parameters for bimodal hydraulic functions
739 by inverse modeling, Soil Sci. Soc. Am. J., 62, 874–880, 1998.
740